Research Article | Vol. 26, No. 10 | 14 May 2018 | OPTICS EXPRESS 12547
Optics EXPRESS

Dielectric metasurfaces in transmission and reflection modes approaching and beyond bandwidth of conventional blazed grating

JIERONG CHENG,[1] SANDEEP INAMPUDI,[2] FEI FAN,[1] XIANGHUI WANG,[1] SHENGJIANG CHANG,[1] AND HOSSEIN MOSALLAEI[2,*]

[1] *Institute of Modern Optics, Nankai University, Key Laboratory of Optical Information Science and Technology, Ministry of Education, Tianjin, 300071, China*
[2] *Department of Electrical and Computer Engineering, Northeastern University, 360 Huntington Ave. Boston, MA 02115, USA*
[*] *hosseinm@ece.neu.edu*

Abstract: Beyond the wave manipulation at a single frequency, efficiency bandwidth control and functional dispersion engineering over metasurfaces are key challenges towards practical applications. Here we propose a type of wideband dielectric metasurfaces made of ultra-thin and layered high-index dielectric patches. The inclusions can be considered as effective material with designable effective refractive index and dispersion. Beam-deflection metasurfaces composed of such inclusions are characterized with the bandwidth approaching and surpassing the limit of conventional blazed gratings in transmission and reflection manners. The bandwidths are more than twice of that in popular single-layer dielectric metasurfaces made of pillar and disk building blocks. In addition, the proposed design benefits from operation over wide range of incident angles and with large tolerance to fabrication errors. More complicated beam manipulation can be fulfilled similarly with great potential for wideband planar optics.

OCIS codes: (160.3918) Metamaterials; (050.5080) Phase shift; (050.6624) Subwavelength structures; (310.4165) Multilayer design; (260.2030) Dispersion.

References and links

1. P. Genevet, F. Capasso, F. Aieta, M. Khorasaninejad, and R. Devlin, "Recent advances in planar optics: from plasmonic to dielectric metasurfaces," Optica **4**, 139–152 (2017).
2. S. B. Glybovski, S. A. Tretyakov, P. A. Belov, Y. S. Kivshar, and C. R. Simovski, "Metasurfaces: From microwaves to visible," Phys. Rep. **634**, 1–72 (2016).
3. C. L. Holloway, E. F. Kuester, J. A. Gordon, J. O'Hara, J. Booth, and D. R. Smith, "An overview of the theory and applications of metasurfaces: The two-dimensional equivalents of metamaterials," IEEE Antennas and Propagation Magazine **54**, 10–35 (2012).
4. Y. Zhao and A. Alù, "Manipulating light polarization with ultrathin plasmonic metasurfaces," Phys. Rev. B **84**, 205428 (2011).
5. X. Ni, A. V. Kildishev, and V. M. Shalaev, "Metasurface holograms for visible light," Nature Communications **4**, 2807 (2013).
6. E. Maguid, I. Yulevich, D. Veksler, V. Kleiner, M. L. Brongersma, and E. Hasman, "Photonic spin-controlled multifunctional shared-aperture antenna array," Science **352**, 1202–1206 (2016).
7. S. Chen, F. Fan, X. Wang, P. Wu, H. Zhang, and S. Chang, "Terahertz isolator based on nonreciprocal magneto-metasurface," Opt. Express **23**, 1015–1024 (2015).
8. J. Cheng, S. Inampudi, and H. Mosallaei, "Optimization-based dielectric metasurfaces for angle-selective multifunctional beam deflection." Sci. Rep. **7**, 12228 (2017).
9. N. Yu, P. Genevet, M. A. Kats, F. Aieta, J.-P. Tetienne, F. Capasso, and Z. Gaburro, "Light propagation with phase discontinuities: generalized laws of reflection and refraction," Science **334**, 333–337 (2011).
10. A. Arbabi, Y. Horie, A. J. Ball, M. Bagheri, and A. Faraon, "Subwavelength-thick lenses with high numerical apertures and large efficiency based on high-contrast transmitarrays," Nature Communications **6**, 7069 (2015).
11. M. Khorasaninejad, W. T. Chen, R. C. Devlin, J. Oh, A. Y. Zhu, and F. Capasso, "Metalenses at visible wavelengths: Diffraction-limited focusing and subwavelength resolution imaging," Science **352**, 1190–1194 (2016).
12. R. Paniagua-dominguez, Y. F. Yu, E. Khaidarov, S. Choi, V. Leong, R. M. Bakker, X. Liang, Y. H. Fu, V. Valuckas, L. A. Krivitsky, and A. I. Kuznetsov, "A metalens with near-unity numerical aperture," Nano Letters **18**, 2124–2132

#321414 https://doi.org/10.1364/OE.26.012547
Journal © 2018 Received 5 Feb 2018; revised 20 Apr 2018; accepted 20 Apr 2018; published 2 May 2018

Optics EXPRESS

(2018).
13. G. Zheng, H. Mühlenbernd, M. Kenney, G. Li, T. Zentgraf, and S. Zhang, "Metasurface holograms reaching 80% efficiency," Nature Nanotechnology **10**, 308–312 (2015).
14. E. Cambril, H. Launois, P. Lalanne, P. Chavel, and S. Astilean, "Design and fabrication of blazed binary diffractive elements with sampling periods smaller than the structural cutoff," J. Opt. Soc. Am. A **16**, 1143–1156 (1999).
15. Z. L. Mei, J. Bai, and T. J. Cui, "Gradient index metamaterials realized by drilling hole arrays," J. Phys. D: Applied Physics **43**, 055404 (2010).
16. M. Li and N. Behdad, "Wideband true-time-delay microwave lenses based on metallo-dielectric and all-dielectric lowpass frequency selective surfaces," IEEE Transactions on Antennas and Propagation **61**, 4109–4119 (2013).
17. J. Cheng and H. Mosallaei, "Truly achromatic optical metasurfaces: a filter circuit theory-based design," J. Opt. Soc. Am. B **32**, 2115–2121 (2015).
18. Y. Li, I. Liberal, and N. Engheta, "Dispersion synthesis with multi-ordered metatronic filters," Opt. Express **25**, 1937–1948 (2017).
19. S. DR, V. DC, K. T, and S. CM, "Electromagnetic parameter retrieval from inhomogeneous metamaterials." Phys. Rev. E **71**, 036617 (2005).
20. E. Arbabi, A. Arbabi, S. M. Kamali, Y. Horie, and A. Faraon, "Multiwavelength polarization-insensitive lenses based on dielectric metasurfaces with meta-molecules," Optica **3**, 628–633 (2016).
21. J. Cheng, D. Ansari-Oghol-Beig, and H. Mosallaei, "Wave manipulation with designer dielectric metasurfaces," Opt. Lett. **39**, 6285–6288 (2014).
22. M. Decker, I. Staude, M. Falkner, J. Dominguez, D. N. Neshev, I. Brener, T. Pertsch, and Y. S. Kivshar, "High-efficiency dielectric huygens' surfaces," Adv. Opt. Mater. **3**, 813–820 (2015).
23. Y. F. Yu, A. Y. Zhu, R. Paniagua-Dominguez, Y. H. Fu, B. Luk'Yanchuk, and A. I. Kuznetsov, "High-transmission dielectric metasurface with 2π phase control at visible wavelengths," Laser Photonics Reviews **9**, 412–418 (2015).
24. R. Bräuer and O. Bryngdahl, "Design of antireflection gratings with approximate and rigorous methods," Appl. Opt. **33**, 7875–7882 (1994).
25. G. J. Swanson, "Binary optics technology: The theory and design of multi-level diffractive optical elements," MIT Technical Report **854** (1989).
26. M. Moharam, E. B. Grann, D. A. Pommet, and T. Gaylord, "Formulation for stable and efficient implementation of the rigorous coupled-wave analysis of binary gratings," J. Opt. Soc. Am. A **12**, 1068–1076 (1995).
27. S. Inampudi, D. Adams, T. Ribaudo, D. Slocum, S. Vangala, W. Goodhue, D. Wasserman, and V. Podolskiy, "ε-near-zero enhanced light transmission through a subwavelength slit," Physical Review B **89**, 125119 (2014).
28. S. Liu, M. B. Sinclair, S. Saravi, G. A. Keeler, Y. Yang, J. Reno, G. M. Peake, F. Setzpfandt, I. Staude, and T. Pertsch, "Resonantly enhanced second-harmonic generation using iii-v semiconductor all-dielectric metasurfaces," Nano Letters **16**, 5426–5432 (2016).
29. S. Liu, G. A. Keeler, J. L. Reno, M. B. Sinclair, and I. Brener, "III-V semiconductor nanoresonators - new strategy for passive, active, and nonlinear all-dielectric metamaterials," Adv. Opt. Mater. **4**, 1457–1462 (2016).
30. C. Sauvan, P. Lalanne, and M.-S. L. Lee, "Broadband blazing with artificial dielectrics," Opt. Lett. **29**, 1593–1595 (2004).
31. C. Ribot, M.-S. L. Lee, S. Collin, S. Bansropun, P. Plouhinec, D. Thenot, S. Cassette, B. Loiseaux, and P. Lalanne, "Broadband and efficient diffraction," Adv. Opt. Mater. **1**, 489–493 (2013).
32. E. Arbabi, A. Arbabi, S. M. Kamali, Y. Horie, and A. Faraon, "Controlling the sign of chromatic dispersion in diffractive optics with dielectric metasurfaces," Optica **4**, 625-632 (2017).
33. S. Wang, P. C. Wu, V.-C. Su, Y.-C. Lai, M.-K. Chen, H. Y. Kuo, B. H. Chen, Y. H. Chen, T.-T. Huang, J.-H. Wang *et al.*, "A broadband achromatic metalens in the visible," Nature nanotechnology **13**, 227 (2018).
34. W. T. Chen, A. Y. Zhu, V. Sanjeev, M. Khorasaninejad, Z. Shi, E. Lee, and F. Capasso, "A broadband achromatic metalens for focusing and imaging in the visible," Nature nanotechnology p. 1 (2018).

1. Introduction

Motivated by device minimization and integration, metasurfaces are experiencing extremely fast progress in control and transformation of electromagnetic waves from microwave to visible spectrum [1–3] with diverse functionalities [4–8]. Subwavelength inclusions offer desired local phase shift to relax the traditional Snell's law [9] and show large freedom to tailor the wavefront as desired. Laboratory demonstrations of some metadevices have been done with comparable or even superior performance compared to the conventional optical elements, such as diffraction-limited high numerical-aperture focusing [10–12] and high-efficiency holographic imaging [13]. Still essential efforts are needed towards engineering the functional dispersion and enlarging the bandwidth.

The functional dispersion describes variation of a certain feature with wavelength, such as the wavelength dependence of the deflection angle in metagratings. The linear phase function

Optics EXPRESS

in a metagrating is implemented by folding the phase spatially into multiple 2π zones with respect to the center frequency. The invariance of the zone boundary with frequency leads to the well-known diffractive dispersion that separates different frequencies.

In contrast, the working bandwidth in terms of the efficiency spectrum is mainly determined by the structure dispersion of the metasurface inclusions. Ideally, if the inclusion offers a constant phase delay regardless of frequency, i.e. $\phi(\omega) = \frac{\omega L}{c} n_{eff}(\omega) - \phi_0(\omega) = const.$, the device efficiency can be maintained over the spectrum. Here n_{eff} and L are the effective refractive index and the thickness of the inclusion; ω is the angular frequency; $\phi_0(\omega)$ is an additional phase term for all the inclusions. Please note that in such case the functionality of the device is still dispersive. Waves with different frequencies are diffracted into different directions but with the same efficiency as along as the diffraction order exists. If $\phi_0(\omega)$ is neglected, anomalous structure dispersion $\frac{dn_{eff}}{d\omega} < 0$ is required, which is quite challenging over a wide bandwidth. Most of the dielectric materials show normal dispersion ($\frac{dn}{d\omega} > 0$) or zero dispersion ($\frac{dn}{d\omega} = 0$), leading to a finite bandwidth for surface-relief blazed gratings. Subwavelength resonators exhibit increased normal dispersion around the resonances, which further narrow the bandwidth when arranged together as a metagrating. Metasurfaces based on effective medium show the lowest structure dispersion, but relying on demanding fabrication requirement of extremely high aspect ratio [14, 15].

In this work, we keep the diffractive functional dispersion and propose a design with wide efficiency bandwidth by engineering the structure dispersion in metasurfaces utilizing low-aspect-ratio layered configuration with total thickness of $\lambda/3$. The efficiency bandwidth of the transmission design and the reflection design approaches and surpasses that of conventional blazed grating made of dispersionless materials, respectively, which is more than twice as large as that of popular dielectric metasurfaces made of thick pillars and thin disks. The thinness and the off-resonance feature offer additional merits of wide range of incident angles and large dimension-error tolerance.

2. Layered phase shifters

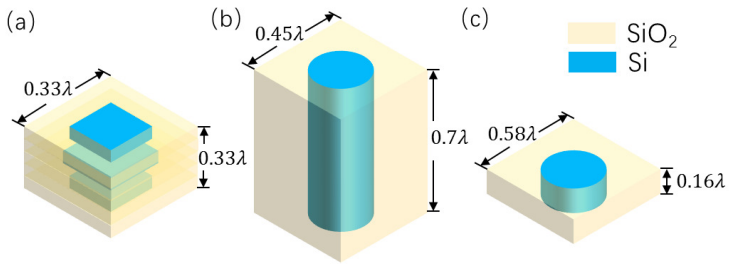

Fig. 1. (a) The layered inclusion studied in this work and the designs using dielectric thick pillar (b) and thin disk (c). The periodicity and the thickness information is marked relative to the center wavelength.

The transmission phase shifters are composed of three-layer ultra-thin high-index dielectric patches separated by low-index host medium in Fig. 1(a) with the total thickness around $1/3$ of the center wavelength. The high-index and low-index materials are chosen as Si and SiO_2, respectively. With proper design of the thickness of each layer and the dimensions of Si patches, it has been shown with low-pass response and true time delay [16–18] in a certain bandwidth. The effective refractive index n_{eff} is retrieved from the transmission coefficient T of the periodic

Optics EXPRESS

element array by [19]

$$T = \frac{2}{2cos(\phi) + j(\eta + \frac{1}{\eta})sin(\phi)} \tag{1}$$

where $\phi = n_{eff}k_0L$, $\eta = n_b/n_{eff}$, with $n_b = \sqrt{2.2}$ as the refractive index of the background SiO_2, k_0 as the vacuum wave number, and L as the total thickness. The effective permeability is assumed to be 1. The phase shifter and an equivalent homogeneous layer with the same thickness and the refractive index of n_{eff} have the same transmission response.

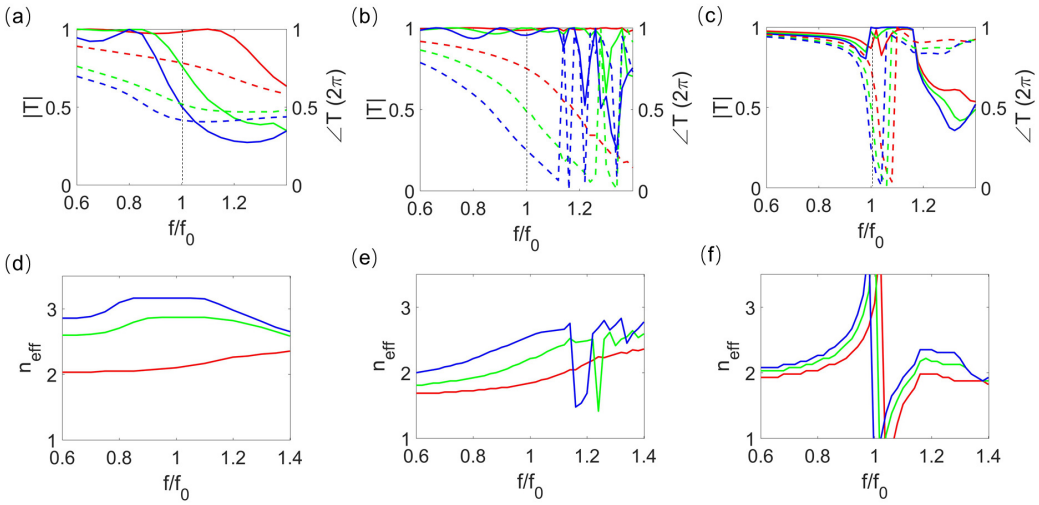

Fig. 2. Transmission spectrum of phase shifters made of layered structures (a), pillars (b), and disks (c). The solid lines are for amplitude and dash lines for phase. Different elements are represented by different colors. (d)-(f) Variation of the effective refractive index of the inclusions with frequency retrieved from the responses in (a)-(c). Only real part is considered.

Next, we choose two types of popular dielectric inclusions: thick pillars [10, 20] [Fig. 1(b)] and thin disks [21–23] [Fig. 1(c)] as the based designs for comparison. Comparison of them with the layered inclusion is done when they offer the same phase delay of $[\frac{\pi}{2}, \pi, \frac{3\pi}{2}]$ at the center frequency f_0 by properly choosing the dimensions of Si pattern. All of them are composed of Si patterns embedded in SiO_2. The fixed periodicity and the thickness are marked in Fig. 1 following the literature report. The layered inclusion is still thin compared to the other two single-layer designs. Since they are studied at different frequencies in literature, the layered one at 600 nm [17], and the other two at 1.55μm [10, 21], the layered one is scaled to work around 1.55μm, and normalization relative to the center frequency is done throughout this work for clarity.

Table 1. **Diameters of phase shifters normalized to λ_0**

unit cell	1	2	3
layer	[0.23 0.22 0.23]	[0.3 0.32 0.3]	[0.33 0.33 0.33]
pillar	0.18	0.22	0.27
disk	0.31	0.34	0.36

The frequency responses of different types of elements are summarized in Fig. 2(a)-2(c). Three

pillar elements in Fig. 2(b) and three disk elements in Fig. 2(c) show transmission phase of $[0.75, 0.5, 0.25]2\pi$ respectively with high transmission at the center frequency, where the phase is relative to the case without Si patterns. The transmission phase in the layered element covers only 1.2π due to the limited thickness, So elements with $[0.75, 0.5, 0.4]2\pi$ responses are plotted in Fig. 2(a). One can improve the phase range by adding more layers of Si patches, which is not considered in this work due to the increased structure complexity. The diameters for all the 9 elements are shown in Table. 1, where each layered element has three diameters (side length) corresponding to three Si patches along the propagation direction. The thickness for each layer is $[55, 68, 100, 68, 55]$nm respectively, and fixed throughout all the layered transmission designs considering the fabrication constraints.

The effective refractive index is retrieved for each element using Eq. (1) and summarized in Fig. 2(d)-2(f). The layered element has most flat effective index over frequency with minimum structure dispersion among the three plots. It is dispersionless around the center frequency, and has small normal dispersion at lower frequencies and small anomalous dispersion at higher frequencies. Variation of n_{eff} increases in the pillar element with increased slope and additional oscillations, and it becomes strongest in the disk one with a strong oscillation around the center frequency. Please note, if the layered inclusion is replaced by a single layer configuration with the same thickness and the same periodicity, it can offer the same phase delay, but with much larger structure dispersion. The layered configuration offers additional freedom to tailor the structure dispersion to the needs. Material dispersion of Si is taken into account through this work. Since Si shows low dispersion around 1.55μm, the variation of n_{eff} in Fig. 2(d)-2(f) is mainly from the structure dispersion.

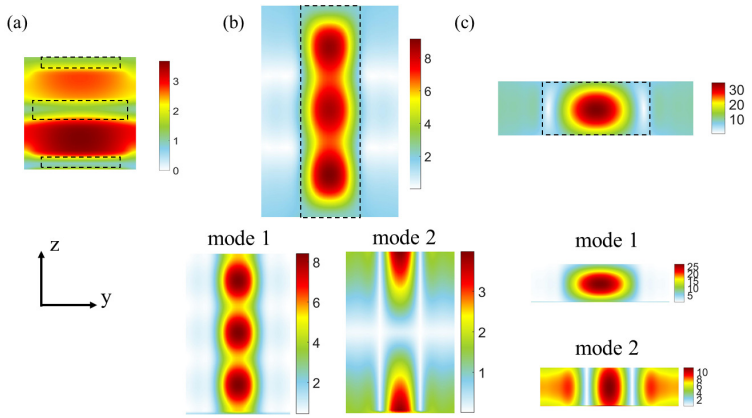

Fig. 3. (a) Field profile in the layered π phase shifter. (b) Total field profile in the pillar π phase shifter and the two guided modes in it. (c) Total field profile in the disk π element and the two guided modes in it. Magnetic component H_x in the y-z plane is plotted with the excitation of E_y and k_z. The dash lines indicate the edges of the Si patterns.

The structure dispersion is related to the physics of the phase delay and the modes in the elements. The layered elements work as low-pass filters around the passband edge and far from resonances. Figure. 3(a) shows that although the layered configuration is beyond the effective medium (EM) theory [24] considering several layers and the relatively large lattice size of $1/3$ wavelength, the element still behaves closely as homogeneous slab with quite uniform intensity distribution. In contrast, the pillar and the disk exhibit much stronger field enhancement in Fig. 3(b) and 3(c) as shown by the colorbar. The pillar works as a waveguide with 2 guided modes. The disk works on the resonances where magnetic resonance (mode 1) and electric resonance (mode 2) are spectrally overlapped with large transmittance [21].

Optics EXPRESS

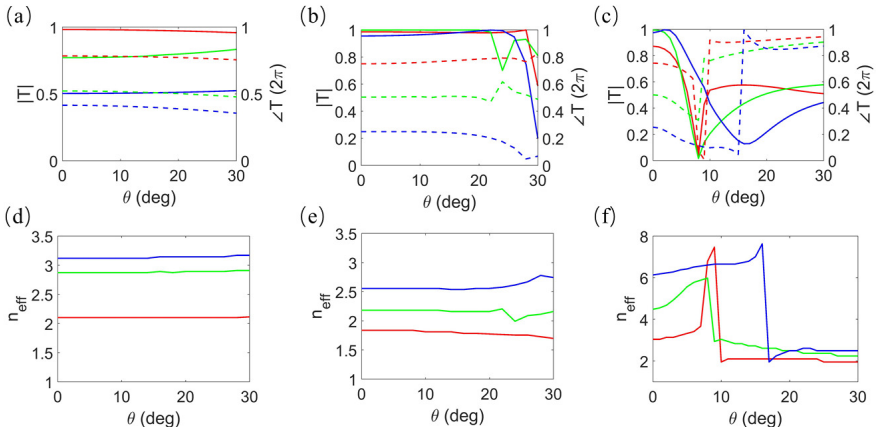

Fig. 4. (a-c) Angular response of the layered, pillar and disk inclusions. The solid lines are for amplitude and dash lines for phase. Different elements are represented by different colors. (d-f) Effective refractive index as a function of the incident angle.

In the pillar and disk designs, they both support two guided modes, as the high transmittance and the π phase shift cannot be achieved within the single-mode regime. The two modes propagate along z direction and interact through the top and the bottom interfaces to offer the desired response. The optimum interaction can be guaranteed only at a specific frequency through dimension design, being out of control at other nearby frequencies, leading to increased structure dispersion.

The angular responses of the same phase shifters as in Fig. 2 are summarized in Fig. 4(a)-4(c) when the incident beam comes from different directions. The layered element is not sensitive to the angle up to 30°; the pillar maintains the response up to around 20°; the disk element changes its transmission rapidly with angle. In Fig. 4(d)-4(f), n_{eff} is retrieved using Eq. (1) with modified $\phi = \sqrt{n_{eff}^2 - n_b^2 sin^2(\theta)} k_0 L$ and $\eta = \frac{n_b cos(\theta)}{\sqrt{n_{eff}^2 - n_b^2 sin^2(\theta)}}$, where θ is the incident angle.

3. Bandwidth of metadevices for beam deflection

The phase shifters analyzed above are representatives to show the structure dispersion of different types of inclusions. Here we study the bandwidth of metasurfaces composed of the above three types of inclusions when the beam is deflected from normal direction into 15° for fair comparison. The length of the supercell Λ is calculated to be $2.6\lambda_0$ with λ_0 as the center wavelength using the well-known grating equation [9]. The layered supercell consists of 8 phase shifters. The pillar and disk supercells are composed of 5 phase shifters. They are schematically illustrated in Fig. 5(a).

The phase excursion in a supercell can be expressed as $\Delta\Phi = \frac{\omega L}{c}[n_M(\omega) - n_m(\omega)]$, where n_M and n_m are the maximum and the minimum effective refractive index at the two ends of the supercell. $\Delta\Phi$ is 2π at f_0 by design with ideally unity efficiency. The decrease of the efficiency at other frequencies is determined by how fast $\Delta\Phi$ is deviated from 2π, which is ultimately controlled by the dispersion of n_M and n_m. Usually n_m is dispersionless by using low-index background without any pattern. If other elements are made of dispersionless effective material as well, $\Delta\Phi \propto \omega$, the efficiency spectrum of such grating follows [25]

$$E = sinc^2(1 - \frac{f}{f_0}) \tag{2}$$

It is illustrated in Fig. 5(b) as the solid line with the half-power bandwidth of 80%. Increasing and

Optics EXPRESS

decreasing this bandwidth is possible by engineering n_M with anamolous and normal dispersion, respectively.

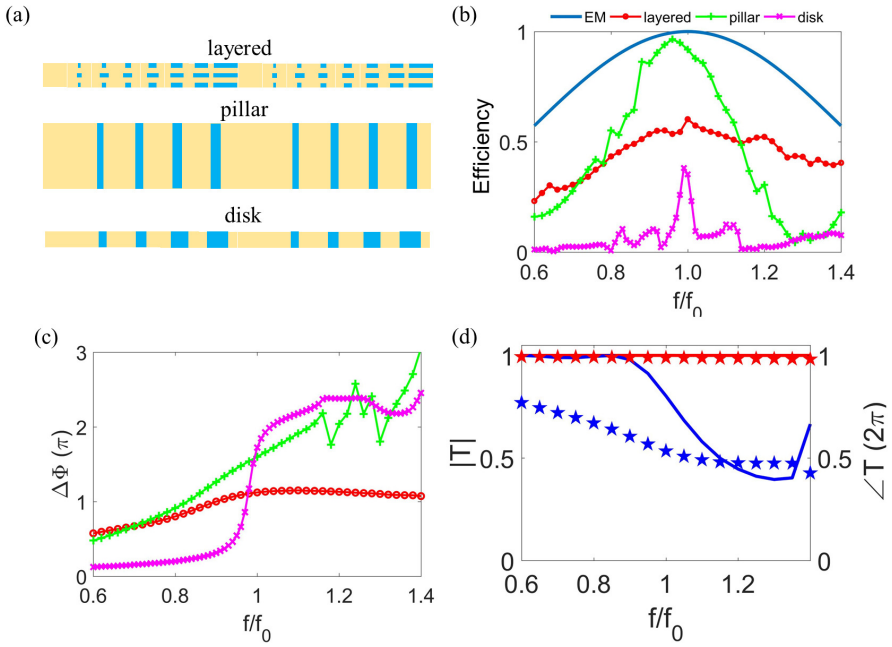

Fig. 5. (a) Schematic illustration of the three metasurfaces by repeating two supercells in each. (b) Efficiency spectrum of the metasurfaces for 15° beam deflection. Solid line is from Eq. (2). Dot line, plus line and cross line are for layered, pillar and disk metasurfaces, respectively. (c) Variation of $\Delta\Phi$ in the supcercell over frequency with the same legend as in (b). (d) Transmission amplitude and phase of the first (red) and the last elements (blue) in the layered supercell. Solid lines are amplitude and star markers are phase.

The bending efficiency, defined as the energy fraction diffracted into the 1^{st} order of the supercell relative to the input energy, is plotted in Fig. 5(b) for metasurfaces made of three types of inclusions. The calculation is done with Rigorous Coupled-Wave Analysis using the formulations in literature [26, 27]. The efficiency spectrum shows that the layered metasurface outperforms the other two in terms of the bandwidth. The half-power bandwidth is 76%, 35% and 5% for layered, pillar and disk metasurfaces, respectively. The bandwidth of the layered metasurface is very close to the theoretical bandwidth of the grating made of dispersionless material, which is consistent with the dispersion analysis of the elements in Fig. 2. However, the peak efficiency is 0.6, 0.92 and 0.38 for the layered, pillar and disk designs, respectively. The layered design scarifies around 30% peak efficiency to gain around 30% bandwidth compared to the pillar structures. The relative low efficiency of the layered design comes from the limited phase shift of 1.2π and non-unity transmission of the elements. The disk metasurface is a very narrowband design, as it relies on the spectral overlapping of two modes, which happens only at a specific frequency.

The supercell phase excursion $\Delta\Phi$ over frequency is compared for three metasurfaces in Fig. 5(c). Obviously, for layered supercell, the variation of $\Delta\Phi$ is small which agrees with the wide bandwidth. And $\Delta\Phi$ is only around π which limits the peak efficiency of the layered design. $\Delta\Phi$ in the pillar and the disk supercells both achieve 1.6π due to the phase discretization, but only at the center frequency. The larger the slope of $\Delta\Phi$ is, the narrower the bandwidth will be.

Figure. 5(c) shows that $\Delta\Phi$ of the layered supercell is extremely flat from f_0 to $1.4f_0$, from

Optics EXPRESS

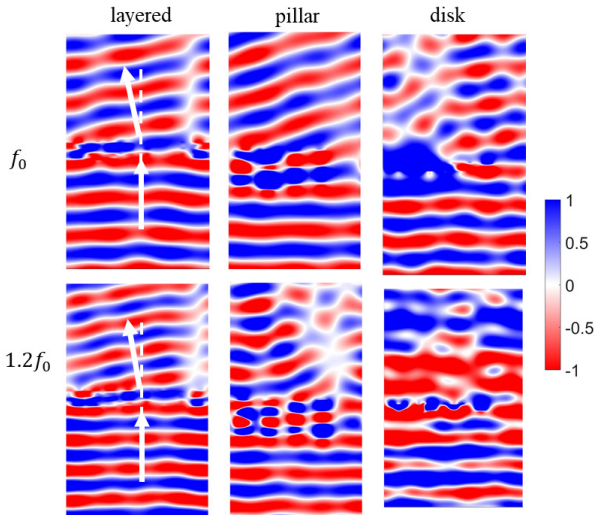

Fig. 6. Beam deflection in layered, pillar and disk metasurfaces at the center frequency f_0 and $1.2f_0$. Real part of H_x is plotted before and after the metasurface supercell.

where we expect that the efficiency should be constant over such frequency range. However, it is not the case in Fig. 5(b). The reason is the non-uniform transmission magnitude. As seen from Fig. 5(d), the phase curves of the first and the last elements in the supercell are parallel to offer the constant $\Delta\Phi$ from f_0 to $1.4f_0$. But the magnitude of the last element is quite low in this frequency range, which explains the decrease of the efficiency. Still one can see the asymmetry of the efficiency spectrum which is larger in the high frequency end. If $\Delta\Phi$ can be maintained without sacrificing the magnitude, the bandwidth can be further improved. Therefor, Eq. (2) is not the fundamental limit of the efficiency spectrum.

The near field profile is shown in Fig. 6 for beam deflection in the three designs at the center frequency f_0 and $1.2f_0$. Real part of the H_x component is plotted within a lateral dimension of a supercell. The pillar design shows the best performance at f_0, while the layered one behaves best at $1.2f_0$.

Variation of the deflection efficiency with the incident angle is studied in Fig. 7(a). The efficiency of pillar and disk metasurfaces drops after 15°. In contrast, the layered metasurface maintains the efficiency of 0.5 even at 45° excitation, approaching the angular response limit of the effective medium design. Since thicker designs usually show worse angular responses, the result of the effective medium design is obtained by simulating a gradient-index slab with the same thickness as the layered design for fair comparison. Angular responses are further validated in Fig. 7(b) by the near field distribution when excitation beam comes from 45°. The theoretical transmission angle is calculated to be 20°, and the result in the layered design shows a good agreement. In contrast, light is scattered into multiple directions with the interference field pattern in the pillar and disk designs.

4. Effects of fabrication errors

A variety of inaccuracy and defects may be introduced inevitably during the fabrication, especially for the layered design with increased number of fabrication steps involved. It is of great significance to numerically evaluate the sensitivity of the device to the fabrication errors. Such errors are mainly three types in the layered design: thickness error of each layer, width error of the patches, and the registration error as the lateral displacement among three Si pattern layers.

Optics EXPRESS

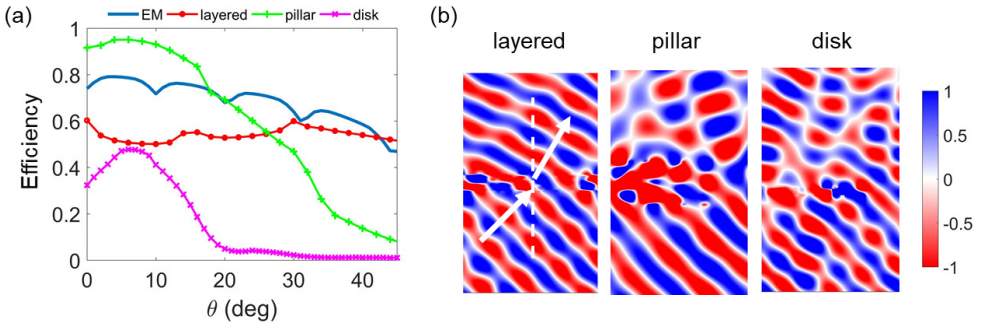

Fig. 7. (a) Angular bandwidth of the metasurfaces. (b) Near field (real part of H_x) in layered, pillar and disk metasurface supercells with 45° excitation.

Figure 8 shows the deflection efficiency when different fabrication errors are introduced. The error is brought with random sign, and the result is averaged for 30 times of calculations. As our expectation, disk designs are very sensitive to the width error and the thickness error. The pillar one is not sensitive to thickness error up to 30nm as it is small relative to the total thickness. Overall, the layered configuration shows large tolerance to all three types of inaccuracy. Especially the thickness error is the error for each layer where 30nm is not small. In addition, the registration is not strictly required within the lattice periodicity. The large tolerance to dimension variation may loose the fabrication requirement in practice.

One possible fabrication procedure is depositing and patterning layer by layer. But it would be challenging to maintain the planar profile. Considering the size of the patches does not change much among the propagation direction in the designs, another way of fabrication could be depositing the high/low index layers alternatively (5 layers in total), and etching them once [28,29]. The registration would not be an issue in this way. If the metasurface can be fabricated in this way with more than 5 layers, the absolute efficiency of the device can be further improved in the transmission mode due to the increased phase response range.

5. Beyond the bandwidth of grating made of dispersionless medium

In order to achieve unity-efficiency deflection over a certain bandwidth, all the elements in a supercell should have parallel phase spectrum with proper phase shift to satisfy $\Delta\Phi(\omega) = 2\pi$. The phase spectrum of the elements can be any shape as long as they keep parallelization (the freedom from $\phi_0(\omega)$ mentioned in Introduction). Examples of ideal phase spectrum of elements at the two ends of the supercell for unity-efficiency deflection is illustrated in Fig. 9. Phase spectrum of

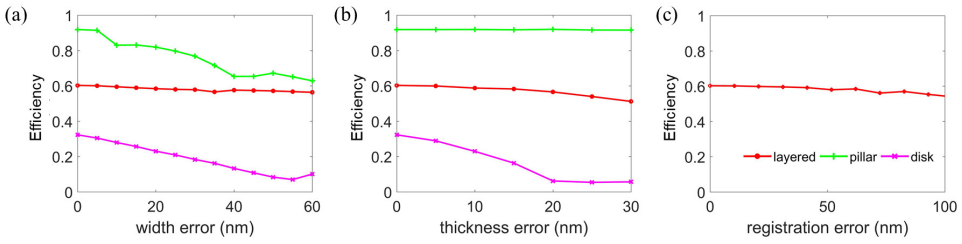

Fig. 8. Beam deflection efficiency of the devices when introducing different amount of the width error (a), the thickness error (b), and the registration error (c) at the center frequency with the normal excitation. The results are averaged for 30 times calculations.

Optics EXPRESS

other elements should keep the same shape and stay in between with equal shift.

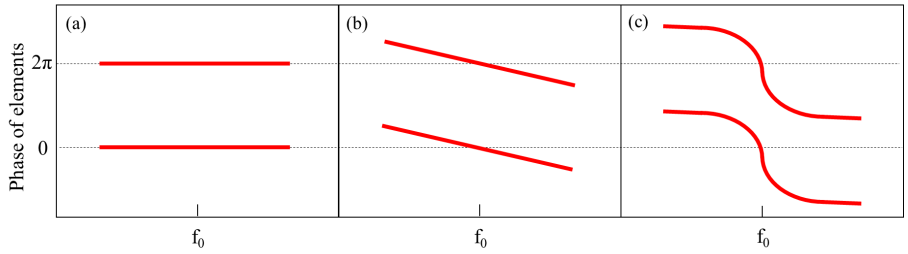

Fig. 9. Examples of ideal phase spectrum of elements at the two ends of the supercell for unity-efficiency deflection.

Throughout this work, the transmission phase is normalized to the one when the inclusion is only background (i.e. $-\frac{\omega n_b L}{c}$). Figure. 9(a) shows a way for wideband operation when all the elements have the same phase shape as that of the background. The above layered design belongs to such case as the first element in a supercell is empty. The designed phase spectrum of the first and the last element is flat and parallel from f_0 to $1.4f_0$. However the small magnitude spectrum decreases the efficiency.

A neat solution to increase the bandwidth using monolayer design has been reported [30, 31]. Instead of fixing the first element in the supercell as the low-index background unit, one can fix the last element in the supercell as the high-index solid unit. As such, the ideal phase spectrum for different elements is Fig. 9(b). From here we can generalize the phase spectrum to other shapes such as Fig. 9(c).

To avoid the magnitude variation and fully utilize the freedom of layered element in the structure dispersion engineering, we next study the layered metasurface in reflection mode. Reflective phase shifters can be designed by adding a metallic substrate in the layered elements. Due to the gained optical path in reflection mode, only two layers of Si patches are needed on top of the mirror in order to achieve complete 2π phase excursion and near unity reflectivity. The typical reflective inclusion is shown in Fig. 10(a). The layers above the mirror can be considered as a homogeneous slab with effective refractive index n_{eff}. Dispersion of n_{eff} can be engineered to achieve the phase spectrum with desired shape.

The reflective metasurface supercell composed of 8 layered phase shifters for 15° beam deflection is designed. Variation of the deflection efficiency over frequency is plotted in Fig. 10(b). The efficiency is above 0.9 from $0.9f_0$ to $1.3f_0$. The bandwidth is beyond Eq. (2). Figure. 10(c) shows the reflection phase spectrum of the 8 supercell inclusions. The first and the last elements are shown with thick red lines, which are parallel over extremely wide frequency range (similar to Fig. 9(b)). The reflection phase spectrum of other elements (thin lines) follow the same shape from $0.9f_0$ to $1.3f_0$, over which near unity efficiency is observed.

The high deflection efficiency is well maintained for large angle of incidence in Fig. 10(d). The angular response of the grating made of dispersionless effective material with the same thickness of 0.3λ on top of the Ag mirror is added in Fig. 10(d) for comparison. Over such small thickness, the refractive index should change spatially in a large range for enough phase delay, which leads to strong impedance mismatch and interference among interfaces. This is the reason of the fluctuation of the efficiency over angle, which also exists in Fig. 7(a). By increasing the thickness of the effective medium layer, the response becomes smooth but more dependent on angle. The near field reflected by the layered metasurface is included in Fig. 10(e) at different frequencies and with different incident angles, which further validates the wideband and wideangle feature of the beam deflection.

Finally, we need to clarify that the direction of the transmitted or reflected beam is 15° only at

Optics EXPRESS

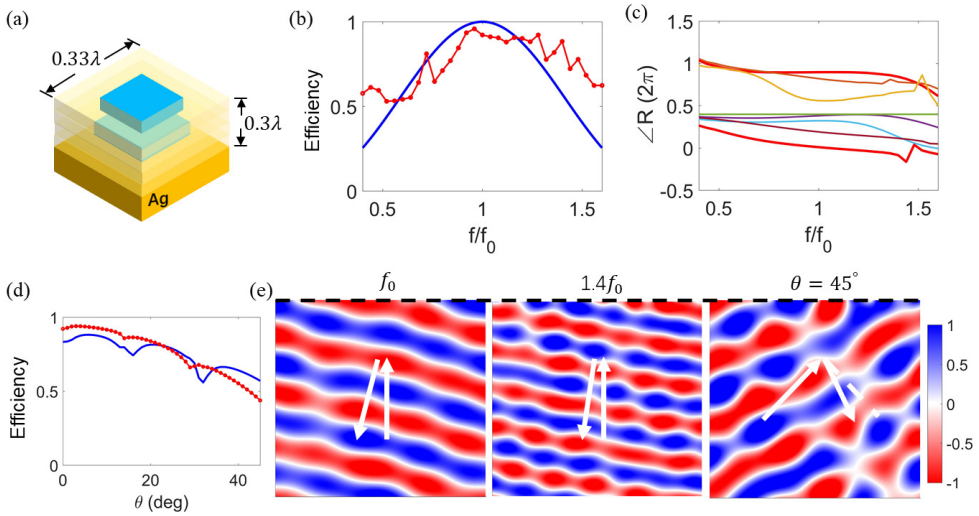

Fig. 10. (a) Geometry of the reflective layered inclusion. (b) Deflection efficiency of the reflective layered design over frequency as the dot line. The solid line is from Eq. (2). (c) Phase spectrum of 8 elements in a supercell. (d) Efficiency for beam deflection over incident angle. Dot line for layered metasurface. Solid line for effective-medium grating with the same thickness. (d) Reflected near field (H_x) by the layered metasurface at different frequencies and with different incident angles. Position of the metasurface is shown as the dash line, and incident field is not shown for clarity.

f_0, and it varies with frequency due to the diffractive dispersion. To achieve achromatic wideband beam deflection, one needs at-will control of both the phase and the dispersion [32–34]. Current design is implemented at several discretized phase points where each phase point has a fixed dispersion. In contrast, achromatic function needs different dispersions at each phase point. The wideband performance here already shows the capability of dispersion engineering especially in the reflective design. The layered metasurfaces will be a potential candidate to achieve achromatic functions.

6. Conclusion

Meta-atoms made of few-layer high-index patches embedded in low-index host are designed for beam deflection over a wide frequency bandwidth and a large range of incident angles. By engineering the structure dispersion, the bandwidth of the transmission metasurface is approaching that of the blazed grating made of dispersionless medium, with the peak efficiency of 0.6. The bandwidth of the reflection metasurface is even larger with peak efficiency above 0.9. Compared to the existing monolayer metasurfaces, the bandwidth is more than doubled. In addition, the designs show good tolerance to the dimension inaccuracy. The study here may shed light on replacing the surface-relief diffractive optics with subwavelength-thin and planar metasurfaces without sacrificing the spectral and angular bandwidth.

Funding

National Natural Science Foundation of China (61671491); National Basic Research Program of China (2014CB339800); Air Force Office of Scientific Research (grant FA9550-14-1-0349).